Proceedings of ASME-JSME-KSME Joint Fluids Engineering Conference 2011
AJK2011-FED
July 24-29, 2011, Hamamatsu, Shizuoka, JAPAN

AJK2011-07020

EXPERIMENTAL INVESTIGATION OF HELICAL CROSS-FLOW AXIS HYDROKINETIC TURBINES, INCLUDING EFFECTS OF WAVES AND TURBULENCE

Peter Bachant
Center for Ocean Renewable Energy (CORE)
University of New Hampshire
Durham, NH, USA

Martin Wosnik
Center for Ocean Renewable Energy (CORE)
University of New Hampshire
Durham, NH, USA

ABSTRACT

The performance characteristics of two cross-flow axis hydrokinetic turbines were evaluated in UNH's tow and wave tank. A 1m diameter, 1.25m (nominal) height three-bladed Gorlov Helical Turbine (GHT) and a 1m diameter, four-bladed spherical-helical turbine (LST), both manufactured by Lucid Energy Technologies, LLP were tested at tow speeds up to 1.5 m/s. Relationships between tip speed ratio, solidity, power coefficient (C_p), kinetic exergy efficiency, and overall streamwise drag coefficient (C_d) are explored. As expected, the spherical-helical turbine is less effective at converting available kinetic energy in a relatively low blockage, free-surface flow.

The GHT was then towed in waves to investigate the effects of a periodically unsteady inflow, and an increase in performance was observed along with an increase in minimum tip speed ratio at which power can be extracted. Regarding effects of turbulence, it was previously documented that an increase in free-stream homogenous isotropic turbulence increased static stall angles for airfoils. This phenomenon was first qualitatively investigated on a smaller scale with a NACA0012 hydrofoil in a UNH water tunnel, using an upstream grid turbulence generator and using high frame-rate PIV to measure the flow field. Since the angle of attack for a cross-flow axis turbine blade oscillates with higher amplitude as tip speed ratio decreases, any delay of stall should allow power extraction at lower tip speed ratios. This hypothesis was tested experimentally on a larger scale in the tow tank by creating grid turbulence upstream of the turbine. It is shown that the range of operable tip speed ratios is slightly expanded, with a possible improvement of power coefficient at lower tip speed ratios. Drag coefficients at higher tip speed ratios seem to increase more rapidly than in the non-turbulent case.

INTRODUCTION

Cross-flow axis hydrokinetic turbines have the ability to extract useful power from moving water, i.e. rivers and tidal flows, without the need for damming. Cross-flow axis turbine designs can receive flow from any direction, as long as it is approximately perpendicular to the axis of rotation, and do not require yaw control to turn them into the flow, as with in-stream axis turbines. In order to ensure these devices operate at peak efficiency, therefore capturing as much energy as possible, their performance characteristics need to be understood in various types of flow conditions. The work described in this paper compares the performance characteristics of two helical cross-flow axis turbines and explores the effects of progressive surface waves of varying periods and small scale isotropic homogeneous (grid) turbulence. This information provides insight into power output prediction, control, and environmental effects, ultimately providing a means to estimate ideal turbine operating parameters for given inflow conditions at a deployment site.

NOMENCLATURE

α Turbine blade angle of attack.
β Blade force angle from radius.
A_f Turbine frontal area.
A_s Turbine swept area.
c Chord length.
C_d Turbine overall drag coefficient.
C_p Turbine power coefficient.
η_{II} Kinetic exergy efficiency.
F Turbine blade force.
F_d Overall turbine drag.
F_D Turbine blade drag.

F_L Turbine blade lift.
J Turbine polar moment of inertia.
λ Tip speed ratio.
L_s Blade span length.
M Grid mesh width.
N Number of blades.
ρ Fluid density.
r Turbine radius.
σ Solidity.
T Wave period.
T_b Brake torque.
T_f Fluid torque.
U Free stream velocity.
U_R Blade relative velocity.

Current State of Technology

Cross-flow axis turbine technology was previously explored for wind energy applications. The most prominent type was the Darrieus turbine with two "jump-rope" shape blades (various mathematical shapes were used), which received much attention during the 1980s [1]. At the end of the 1980s the development of these straight-bladed (with respect to azimuth location) cross-flow axis turbines was essentially abandoned, since the large variations in torque, due to large variations in lift as the blade angle of attack varies throughout the rotation, caused structural fatigue failures of the turbines.

In 1995 Alexander Gorlov designed a cross-flow axis turbine with its blades swept helically to help average the periodically unsteady torques inherent in the straight bladed concept [2]. These Gorlov Helical Turbines (GHTs) are practically identical in two dimensions compared to their straight-bladed counterparts. Consequently, Darrieus turbine performance models and experimental observations are relevant.

To date, there is a scarcity of performance data for helical devices in the literature. The limited information available shows Gorlov Helical Turbines to reach efficiencies as high as 35% [3]. Peak efficiencies for smaller straight-bladed Darrieus turbines have been reported around 23% [4], whereas the peak efficiencies of a 17m diameter Darrieus turbine at Sandia National Laboratory were reported to exceed 40% [1].

Lucid Energy Technologies, LLP (Lucid), formerly GCK Technologies (where "G" stood for Gorlov), carried on the development of the GHT, and succeeded with several small-scale installations over the years. Lucid/GCK also provided two prototypes to the Korean Ocean Research and Development Institute (KORDI) for testing in the Uldolmok Tidal Strait [5]. Based on the experience with the Lucid/GCK GHTs, in 2009, KORDI completed their Uldolmok Tidal Current Power Plant, a full scale test project rated at 1MW. The 6.5m/s maximum current speeds are harnessed via two vertical axis helical devices [6]. In the United States, the Ocean Renewable Power Company (ORPC) is using Gorlov Helical Turbines arranged in pairs on either side of a common generator with horizontal axis in a demonstration installation in Eastport, ME [7,8].

Recently, Lucid developed vertical axis spherical-helical turbines to be installed in pipe sections, with the goal to harvest excess energy available in large gravity-fed water pipes, for example in irrigation or wastewater systems. The drop-in installation has been given the name Northwest PowerPipe™ [9]. Since these turbines are installed in a high blockage closed conduit, they are similar to traditional hydropower installations and the efficiency limit for turbines installed in a free stream, also known as the "Betz" limit [1,10] does not apply.

BACKGROUND AND THEORY

One important design parameter for a cross-flow axis hydrokinetic turbine is its solidity. It is defined as the ratio of total blade planform area to swept area, expressed as:

$$\sigma = \frac{NcL_s}{A_s} \tag{1}$$

Where N is the number of blades, c is the chord length perpendicular to the blade span, L_s is the blade span length, and A_s is the turbine swept area. This definition is in contrast to some definitions for straight-bladed devices. For example, Paraschivoiu defines solidity as the ratio of total chord length to radius [1]. This definition is less useful for non-cylindrical devices since their radii vary with height. For this reason, the area ratio definition of Eq. 1 was used here.

Another parameter for helical devices is blade overlap. This is the ratio of how much total blade span is projected onto the circumference of the device's rotation, which is related to helical sweep angle and turbine height.

Relevant non-dimensional turbine performance characteristics include tip speed ratio, drag coefficient, and power coefficient. Tip speed ratio is defined as

$$\lambda = \frac{\omega r}{U} \tag{2}$$

where ω is the angular speed of the device, r is the radius (or maximum radius if not cylindrical), and U is the free stream velocity. Drag coefficient, sometimes called thrust coefficient when discussing in-stream axis turbines or propellers, is the ratio of drag force to dynamic pressure times frontal area, defined as

$$C_d = \frac{F_d}{\frac{1}{2}\rho A_f U^2} \tag{3}$$

where ρ is the fluid density and A_f is the turbine frontal area. Power coefficient is a similar quantity, providing a measure of the hydrodynamic efficiency of the turbine rotor. It is defined as the shaft power removed divided by the available kinetic power in the free stream for an area equal to the turbine's frontal area; expressed as

$$C_p = \frac{T_b \omega}{\frac{1}{2}\rho A_f U^3} \quad (4)$$

where T_b is the brake torque. The parameters σ, λ, C_d, and C_p allow turbines of different size at different flow conditions and operating states to be readily compared.

In an actual turbine installation the electric power, P_e, delivered by a hydrokinetic turbine will be further reduced by the mechanical transmission, bearing and gearbox efficiency η_m and an electrical generator and power conditioning efficiency η_e, as shown in Eq. 5.

$$P_e = C_p \eta_m \eta_e \tfrac{1}{2}\rho A_f U^3 = \eta_{w-w} \tfrac{1}{2}\rho A_f U^3 = \eta_{w-w} P_{available} \quad (5)$$

The product of all three efficiencies is commonly referred to as overall, or "water-to-wire" efficiency, $\eta_{w\text{-}w}$. When evaluating turbine rotors it is appropriate to eliminate gearboxes and generators and measure the hydrodynamic rotor efficiency (mechanical shaft power) directly using the brake torque loading as described in Eq. 4.

Another measure of performance often overlooked is the second law efficiency or kinetic exergy efficiency. Kinetic exergy efficiency is a measure of how well the device converts any kinetic power it removes from the flow into useful shaft power. This could be important information if turbines are to be used in series, or for environmental impact predictions.

Assuming flow through the device is incompressible, isothermal, and upstream and downstream static pressures are equalized, kinetic exergy efficiency is the ratio of useful mechanical power extracted to the total amount of kinetic power removed from the flow, which is directly related to drag using the principles of continuity, conservation of momentum, and conservation of energy. Kinetic exergy efficiency can be expressed in terms of the drag and power coefficients as follows:

$$\eta_{II} = \frac{C_p}{C_d - \frac{1}{4} C_d^{\,2}} \quad (6)$$

Performance in Waves

The presence of a progressive surface wave creates a periodically fluctuating velocity superimposed upon the steady flow. This velocity has a zero mean value, but since cross-flow axis turbines can extract energy from the flow regardless of the direction of the incoming flow, there arises the possibility of capturing the fluid motion associated with the waves. The horizontal or streamwise component of this motion can be derived from linear small-amplitude (Airy) wave theory and written as [11]:

$$u = \frac{gHk}{2\sigma} \frac{\cosh k(h+z)}{\cosh kh} \cos\left(kx + \sigma t\right) \quad (7)$$

Where u is the horizontal velocity, g is gravitational acceleration, k is the wave number, H is wave height, h is depth from equilibrium surface, z is the vertical coordinate, x is the horizontal coordinate, σ is the radian frequency, and t is time.

Delay of Stall in Grid Turbulence

It was shown by Swalwell et al. in 2001 that grid turbulence can delay the static stall angle of an airfoil [12]. An example of hydrofoil performance data for a selection of symmetrical hydrofoils, presented as lift/drag ratio, is shown in Fig. 1 and stall angles can be readily identified (note that stall angle increases with hydrofoil thickness, and also with Reynolds number for each foil type). Below a certain tip speed ratio, the blade angle of attack (calculated by the vector sum of free stream and blade velocity) will exceed its stall angle, and in this condition the hydrodynamic force on the blade is producing little to no useful torque. It is shown in the free body diagrams in Fig. 2. that torque about the rotation axis is the product of the resultant hydrodynamic force, F, and the sine of its angle, β, with the radius, r, of the blade path. In a stalled condition at high angles of attack, β becomes very small and can even turn negative if the ratio of lift to drag is low enough.

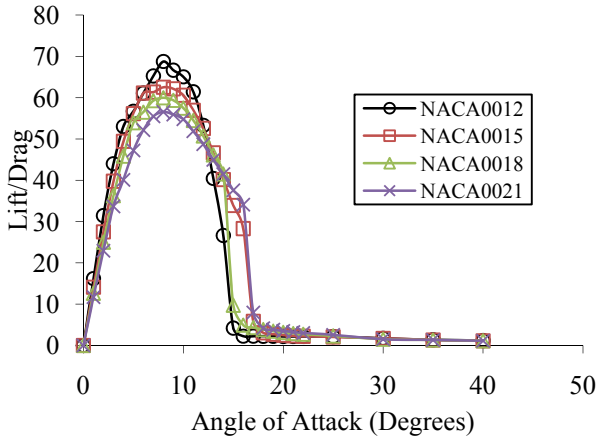

FIGURE 1. LIFT TO DRAG RATIO FOR VARIOUS FOILS (Re=700,000) [12].

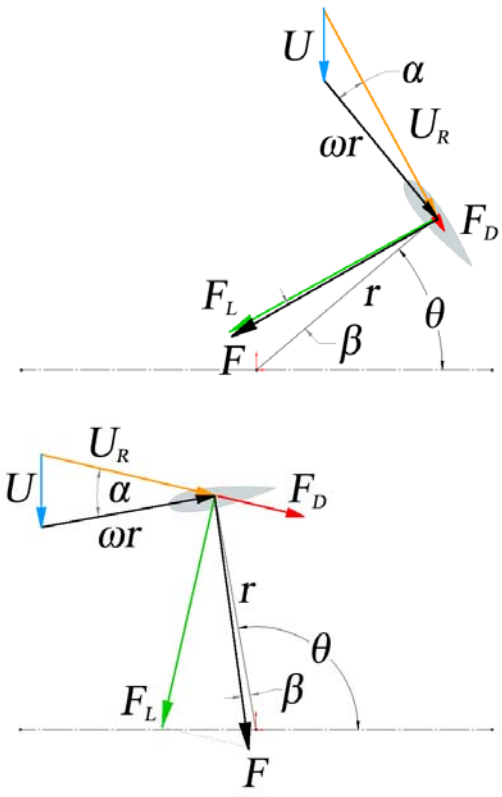

FIGURE 2. SCHEMATICS SHOWING TURBINE BLADE GEOMETRY FOR UNSTALLED (TOP) AND STALLED (BOTTOM) CASE. TIP SPEED RATIO IS 2.5 NEGLECTING INDUCTION AND TURBINE ROTATION IS COUNTER-CLOCKWISE.

Fig. 3 shows the turbine blade angle of attack versus turbine azimuthal angle for a tip speed ratio of 2.4, neglecting induction. Induction, or fractional decrease of free stream velocity as it enters the turbine, reduces angle of attack fluctuation amplitude, and can be thought of as increasing the "local" tip speed ratio seen at the blade. The red dashed lines indicate a typical static stall angle as interpreted from Fig. 1. Note that the amplitude of the angle of attack fluctuation increases as tip speed ratio decreases. If the hydrodynamic torque produced by the blades drops low enough due to excessive stall, the turbine will angularly decelerate if the resistive load torque (from a brake, generator, etc.) remains constant. This deceleration decreases tip speed ratio, worsening the stall condition. This positive feedback cycle ultimately leads to the turbine ceasing rotation altogether.

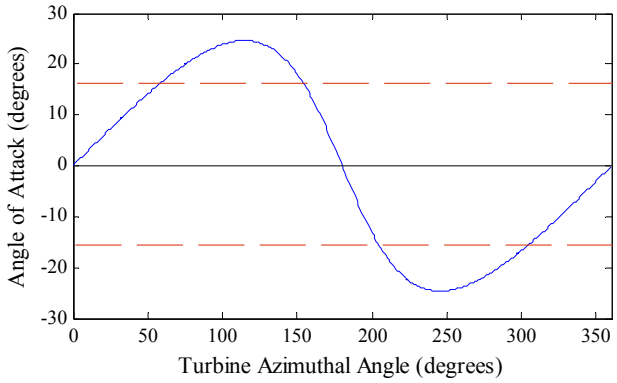

FIGURE 3. TURBINE BLADE ANGLE OF ATTACK CALCULATED FOR TIP SPEED RATIO OF 2.4, NEGLECTING INDUCTION. DASHED HORIZONTAL LINES SHOW TYPICAL STATIC STALL ANGLE.

Since blade angle of attack on the turbine blade is oscillating with turbine rotation, it is important to take into consideration the onset of dynamic stall. Dynamic stall is a more complex phenomenon than static stall and depends mainly on the rate of change of the foil's angle of attack [1]. Dynamic stall has been shown to improve performance in Darrieus wind turbine models. As of yet, any three dimensional effects differentiating helical turbines from straight-bladed turbines are unknown.

Since turbulence has been shown to delay static and dynamic stall [1, 12], it is hypothesized that performance can be enhanced at lower tip speed ratios by introducing grid turbulence upstream of the device.

EXPERIMENTAL SETUP

The UNH Tow & Wave Tank is a 36.6m long, 3.66m wide, 2.44m deep facility capable of towing speeds up to 3m/s (1.5m/s for large models with low gear ratio, 3m/s for smaller models with high gear ratio) and features a flap style wave maker capable of producing waves with 1-5s periods up to 0.4m wave height. The tank was chosen as a platform to develop a hydrokinetic test bed for turbines with frontal areas up to approximately 1.25m^2. Currently, the tow mechanism is being upgraded to allow tow speeds of 2m/s with this size turbine and 3m/s for turbines with half this frontal area.

Turbines

Lucid Energy Technologies, LLP provided two prototypes for testing, their GHT (Gorlov Helical Turbine) and LST (Lucid Spherical Turbine).

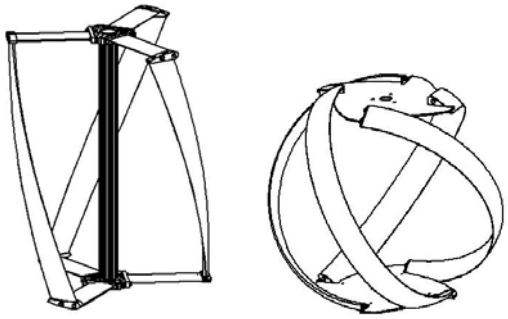

FIGURE 4. GHT (LEFT) AND LST (RIGHT).

TABLE 1. TURBINE SPECIFICATIONS.

	GHT	LST
Diameter (m)	1.00	1.14
Height (m)	1.32	0.97
Blade profile	NACA0020	NACA0020
c (cm)	14	14
σ	0.14	0.22
A_f (m^2)	1.32	0.96
Blade overlap	1/2	2

Fig. 4 shows sketches of the two turbines and Table 1 gives their respective design characteristics. They are comparable in size and construction. However, the GHT is designed for open water environments (ideally to be deployed in flow speeds greater than 1.5m/s) while the LST is designed for use in a constrained circular pipe or conduit; hence it's near-circular frontal projection. There is a notable difference in solidity and blade overlap, the LST having almost twice the solidity and four times the overlap of the GHT. It was of interest to the turbine manufacturer, Lucid, to investigate how the LST performs in an open water environment compared to a similarly sized GHT.

Tow Frame

The turbine tow frame was fabricated from extruded aluminum 14cm chord NACA 0020 struts, also provided by Lucid Energy Technologies, LLP. The goal was to produce the least drag possible to conserve tow power.

Brake torque is provided by a hydraulic disk brake actuated manually by an operator onboard the carriage. The brake master cylinder has an adjustable stop to vary maximum brake pressure, indicated by a mechanical pressure gauge.

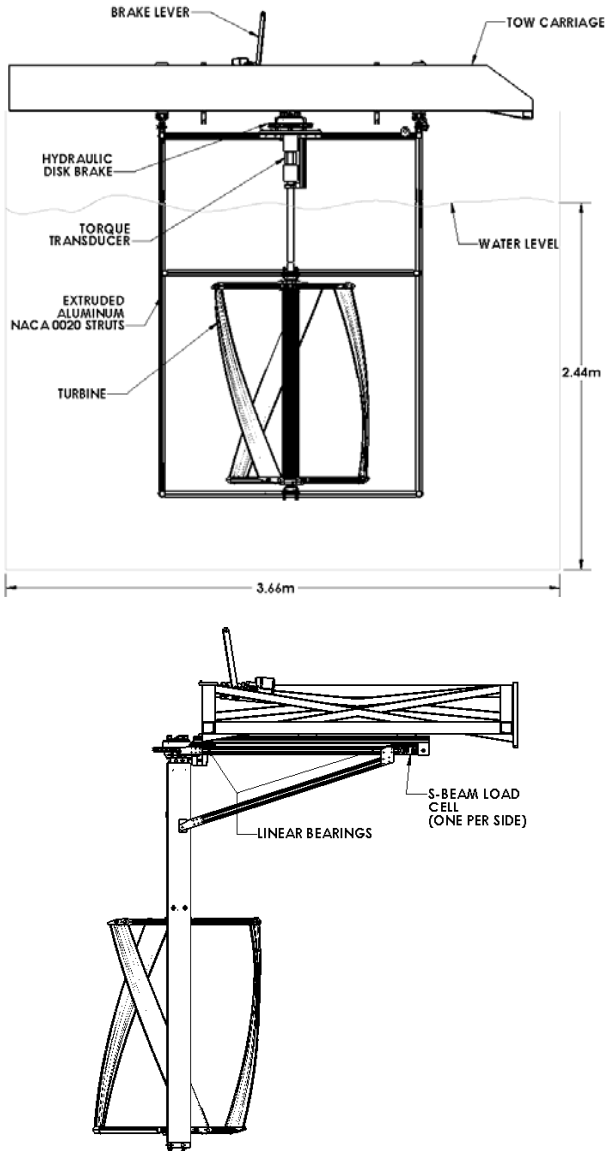

FIGURE 5. TURBINE TEST FRAME OUTLINE FRONT (TOP) AND RIGHT (BOTTOM) VIEWS. TOW DIRECTION IS FROM LEFT TO RIGHT FOR RIGHT VIEW.

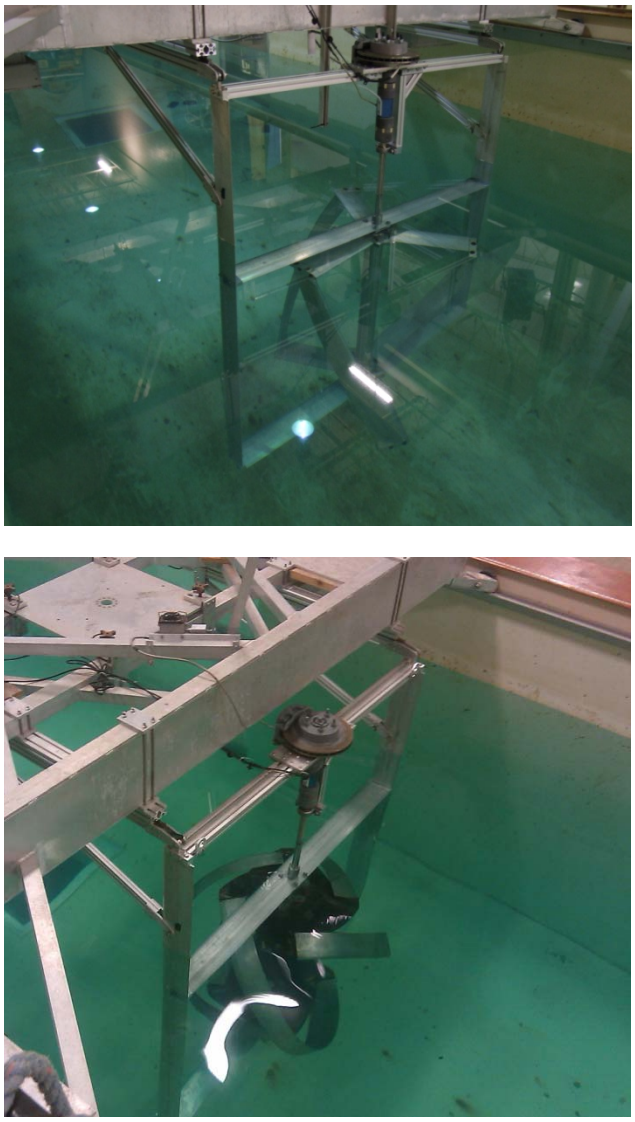

FIGURE 6. THE GHT (TOP) AND LST (BOTTOM) HYDROKINETIC TURBINES INSTALLED IN THE UNH-CORE TURBINE TEST BED.

Instrumentation

Torque is measured by an Interface T8 200Nm torque transducer mounted between the brake and turbine. The uppermost bearing features an integral 54 pulse-per-revolution magnetic pickup used to measure shaft angular speed, whose frequency is measured with a Dataforth DSCA45 frequency signal conditioner. The entire tow frame is mounted to the tow carriage by four precision linear bearing slides allowing streamwise force to be measured by two 500lbf (2224N) capacity Sentran S-beam load cells (one per side). Load cell excitation voltage and signal conditioning is supplied by Dataforth DSCA38 strain gage signal conditioners. Carriage speed is measured by a 60 pulse-per-revolution encoder driven by a 4.8cm diameter wheel, which rides along the main carriage rail. This encoder pulse frequency is measured with a Dataforth DSCA45 frequency signal conditioner. All signals are sampled at 500Hz with a National Instruments USB-6211 DAQ device.

Steady State Measurements

To ensure the measured brake torque is equal to the torque imparted by the fluid, measurements must be taken at constant angular velocity. Eq. 8 shows Newton's Second Law written for a rotating solid body neglecting friction:

$$T_b = T_f - J\dot{\omega} \tag{8}$$

This relation illustrates the need to allow the turbine to reach a steady state to prevent exaggerated measurements caused by the inertial torque associated with angular deceleration.

PIV Experiments

A 15.24cm square water channel was used to perform PIV measurements of a stalling 7cm chord NACA0012 foil with and without grid turbulence, in a free stream velocity of 0.3m/s. The grid used had a 3.18cm mesh width, circular rod cross section, 0.36 solidity, and was mounted 10 mesh widths upstream of the hydrofoil. Images were captured at 500Hz and processed with LaVision DaVis.

Blockage Correction

Since the tow tank represents a constrained flow, actual fluid velocity through the turbine will be slightly exaggerated, inflating power and drag measurements compared to a free flow case. These values are corrected using the process detailed in Appendix A of Bahaj et al., 2006 [14]. This iterative procedure provides a ratio of equivalent free flow velocity to tank velocity based on measured drag coefficient and the ratio of turbine frontal area to tank cross section. The ratio of equivalent free stream velocity to measured free stream velocity is used to correct as follows:

$$\lambda = \lambda_t \left(\frac{U_f}{U} \right) \tag{9}$$

$$C_d = \left(C_d\right)_t \left(\frac{U_f}{U} \right)^2 \tag{10}$$

$$C_p = \left(C_p\right)_t \left(\frac{U_f}{U} \right)^3 \tag{11}$$

where the subscript *"t"* represents values measured in the tow tank and subscript *"f"* denotes the equivalent free flow value. The blockage corrections lowered power coefficients up to 30% for the GHT and 18% for the LST.

RESULTS

Tow Frame Tare Drag and Tare Torque

In order to measure actual turbine drag, tare drag on the frame is measured without a turbine installed. The data is fit with a power law curve and subtracted from turbine measurements. Fig. 7 shows the data plotted against free stream velocity. Since the LST requires two additional shaft extensions compared to the GHT, a separate set of tare drag measurements was performed with those extensions installed.

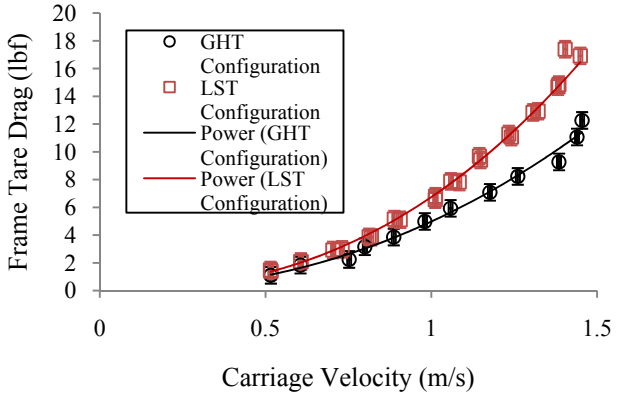

FIGURE 7. TOW FRAME TARE DRAG VERSUS TOW SPEED WITH CORRESPONDING POWER LAW FIT CURVES.

Similarly, friction torque in the bearings below the torque transducer was measured and regressed linearly versus RPM, to be added to the turbine brake torque measurement in post-processing.

Sample Run

Fig. 8 shows a sample data collection run (in arbitrary units, after applying a moving average smoothing filter) for one tow to illustrate how measurements vary with each other and to show a typical steady state duration of interest (16-18s).

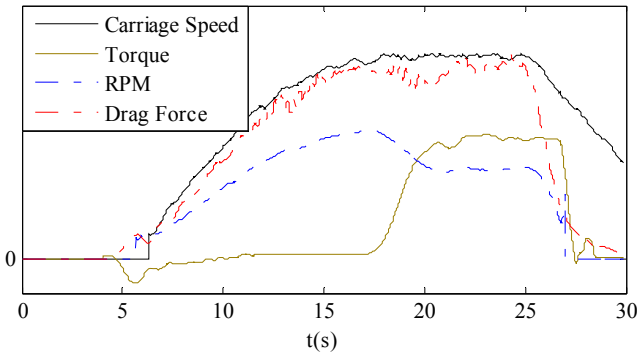

FIGURE 8. SAMPLE DATA COLLECTION RUN SHOWING CARRIAGE SPEED, TURBINE SHAFT RPM, TORQUE, AND OVERALL DRAG FORCE (IN ARBITRARY UNITS).

Measurements are averaged over this region, producing one operating data point. Note that the beginning of the run shows the turbine being started manually, hence the negative torque readings. This is done to help the turbine reach steady state more quickly, since tank length is a limited. It is also done to avoid the high transient drag forces associated with allowing the turbine to self start.

Steady GHT Measurements

Fig. 9 shows the GHT power coefficient plotted versus tip speed ratio. Fig. 10 shows these same values after applying the blockage correction. There appears to be a slight shift toward higher power coefficients and tip speed ratios for higher tow speeds. A maximum blockage-corrected power coefficient of 28% is reached at a tip speed ratio of 2.1. Before blockage correction, a maximum power coefficient of 36% is observed at a tip speed ratio of 2.3. This power coefficient is closer to the 35% reported by Gorlov [3].

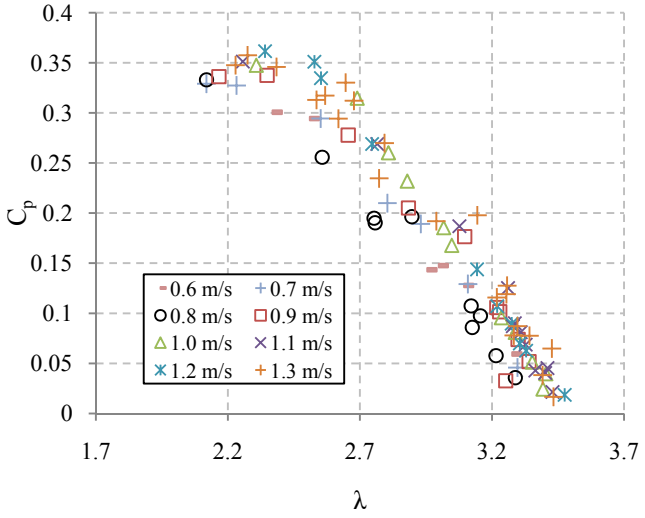

FIGURE 9. GHT POWER COEFFICIENT VERSUS TIP SPEED RATIO BEFORE BLOCKAGE CORRECTION. AVERAGE ERROR FOR C_P = 0.01; FOR λ = 0.04.

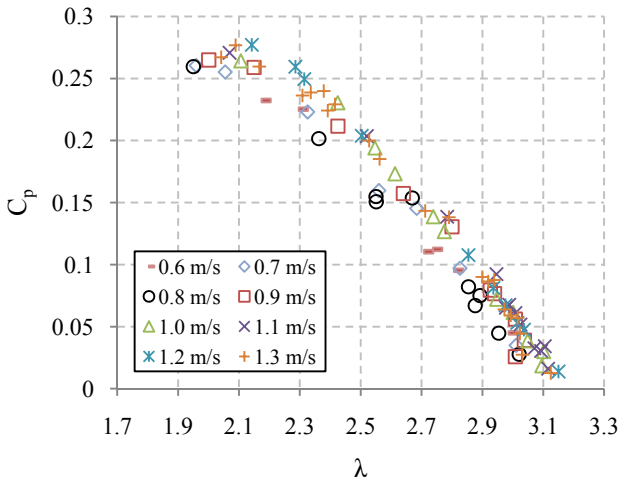

FIGURE 10. BLOCKAGE-CORRECTED GHT POWER COEFFICIENT VERSUS TIP SPEED RATIO. AVERAGE ERROR FOR $C_P = 0.01$; FOR $\lambda = 0.04$.

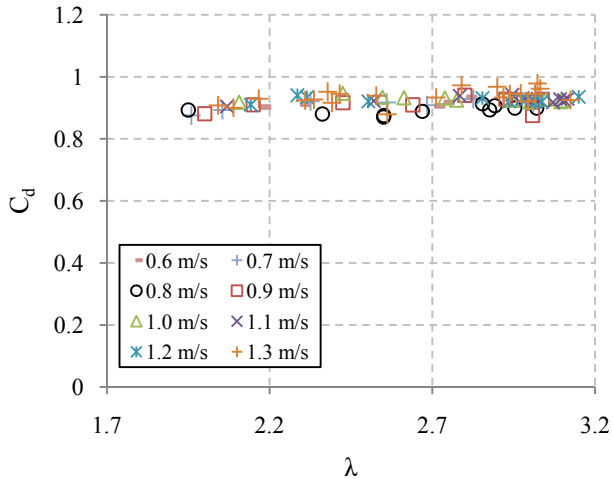

FIGURE 11. BLOCKAGE-CORRECTED GHT DRAG COEFFICIENT VERSUS TIP SPEED RATIO. AVERAGE ERROR FOR $C_d = 0.004$; FOR $\lambda = 0.04$.

Fig. 11 shows blockage-corrected GHT drag coefficient plotted versus tip speed ratio. The values remain quite constant, slightly increasing as tip speed ratio increases. This makes sense since increasing tip speed ratio makes the turbine appear more and more like a solid body. In other words, the likelihood of a fluid particle passing through the device without a reduction in its momentum decreases. It is interesting that the drag on the device remains fairly constant regardless of the power taken out at the shaft. This is useful information for predicting environmental effects of these devices since it implies removal of momentum from the flow whether or not useful shaft power is extracted.

Fig. 12 shows GHT kinetic exergy efficiency versus tip speed ratio (calculated using non-blockage-corrected power and drag coefficients). The curve is similar in shape to the power coefficient curve in Fig. 10. The device reaches a peak kinetic exergy efficiency of 46% at a blockage-corrected tip speed ratio of 2.1.

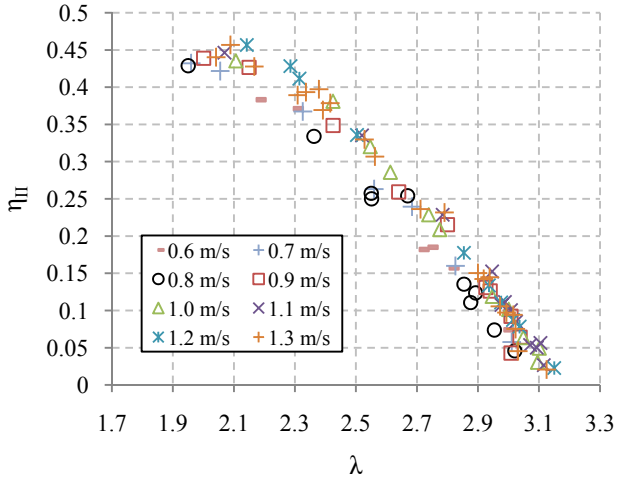

FIGURE 12. GHT KINETIC EXERGY EFFICIENCY VERSUS BLOCKAGE-CORRECTED TIP SPEED RATIO.

Steady LST Measurements

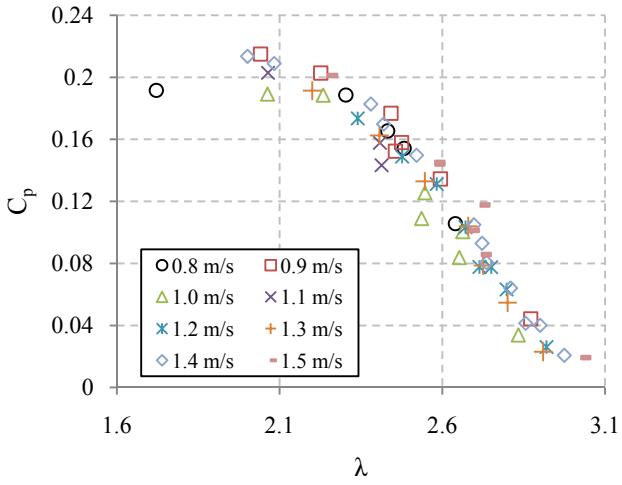

FIGURE 13. BLOCKAGE-CORRECTED LST POWER COEFFICIENT VERSUS TIP SPEED RATIO. AVERAGE ERROR FOR $C_P = 0.01$; FOR $\lambda = 0.03$.

Fig. 13 shows LST power coefficient versus tip speed ratio. Compared with the GHT, power coefficients are lower and the device tends to operate at lower tip speed ratios. Low power can be explained by the device's circular cross section placing blade sections farther from the equator at small radii, therefore lowering local tip speed ratio, increasing local angle of attack fluctuations, thereby inducing stall. This low radius also means blade forces impart a lower moment with respect to the turbine

axis. Tendency to operate at lower tip speed ratios can be attributed to the device's higher solidity, consistent with findings on the operation of the Darrieus wind turbine [1]. Note that the power conversion efficiency of the LST has been measured at up to 46% when installed in a closed conduit of 4 ft (1.22m) diameter [15].

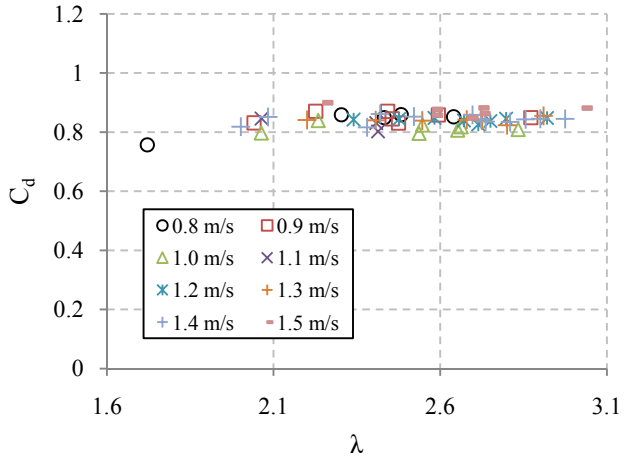

FIGURE 14. BLOCKAGE-CORRECTED LST DRAG COEFFICIENT VERSUS TIP SPEED RATIO. AVERAGE ERROR FOR C_d = 0.002; FOR λ = 0.03.

Fig. 14 shows the LST drag coefficient data plotted against tip speed ratio. Similar to the GHT, the values remain fairly constant with a slight trend toward higher C_d at higher λ. However, the LST overall has a lower drag coefficient. This can be partially attributed to its lack of center shaft.

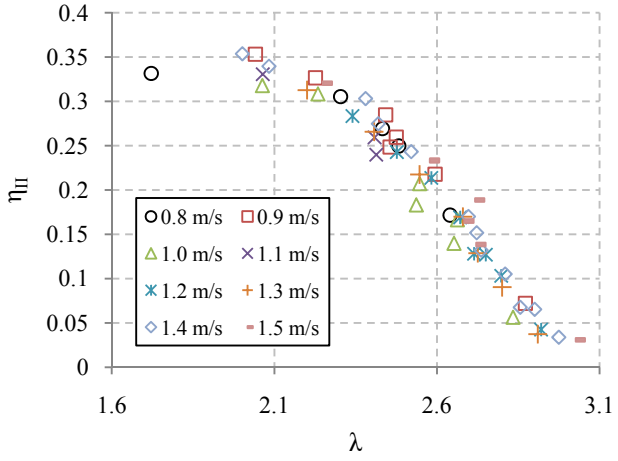

FIGURE 15. LST KINETIC EXERGY EFFICIENCY VERSUS BLOCKAGE-CORRECTED TIP SPEED RATIO.

Fig. 15 shows LST kinetic exergy efficiency plotted versus blockage-corrected tip speed ratio (calculated using non-blockage corrected power and drag coefficients). Like the GHT, kinetic exergy efficiency plotted against tip speed ratio has the same general shape as the power coefficient versus tip speed ratio, and the maximum value corresponds to the tip speed ratio for maximum power coefficient. The LST has a notably lower maximum kinetic exergy efficiency of 35% compared to the GHT's 46%.

GHT Performance in Waves

Turbine performance for the GHT was measured while being towed 1.0-1.1m/s against the direction of propagation of four different types of 0.15m high waves, having periods 1, 1.5, 2, and 2.5s. Fig. 16 shows how the amplitude of the theoretical horizontal wave velocity and particle displacement vary with depth, as calculated from Eq. 7. These parameters averaged over turbine height are shown along with theoretical wavelength in Table 2.

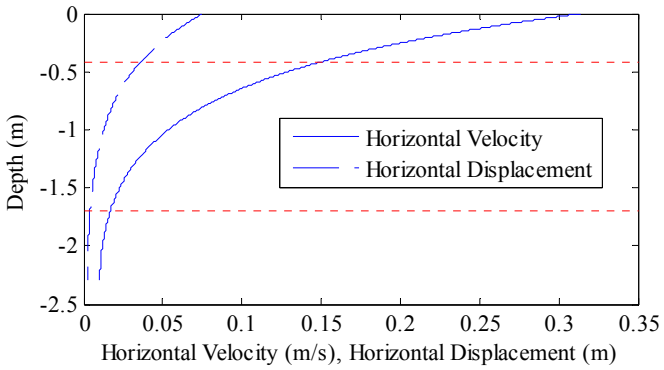

FIGURE 16. THEORETICAL HORIZONTAL WAVE VELOCITY AND DISPLACEMENT AMPLITUDES VERSUS DEPTH FOR A 0.15 METER HIGH, 1.5 SECOND PERIOD WAVE. RED DASHED LINES INDICATE TURBINE POSITION.

TABLE 2. THEORETICAL WAVE PARAMETERS AVERAGED OVER TURBINE HEIGHT.

Period (s)	1.0	1.5	2.0	2.5
Height (m)	0.15	0.15	0.15	0.15
Wavelength (m)	1.6	3.5	6.1	9.0
Horiz. disp. amp. (m)	0.003	0.01	0.03	0.05
Horiz. vel. amp. (m/s)	0.02	0.06	0.09	0.1

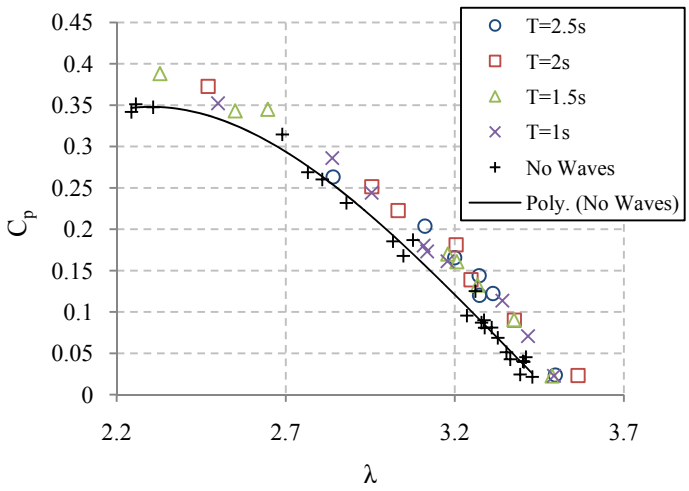

FIGURE 17. GHT POWER COEFFICIENT VERSUS TIP SPEED RATIO FOR U=1.0-1.1m/s WITH AND WITHOUT WAVES. AVERAGE ERROR FOR C_P = 0.01; FOR λ = 0.04.

Fig. 17 shows GHT power coefficient plotted versus tip speed ratio (not corrected for blockage) for carriage speeds of 1.0-1.1m/s. In general, an increase in power coefficient and tip speed ratio is observed towing in waves, including an approximate 11% increase in power coefficient in the 1.5s period wave. With increasing brake torque, the turbine stalled at higher tip speed ratios in waves than in steady flow. For the longest wave period, 2.5s, the turbine stalled at a much higher tip speed ratio than usual. This can be explained when the theoretical wave velocity is included in the calculation of turbine blade angle of attack. Fig. 18 shows the theoretical angle of attack assuming a 30% induction (this is close to the induction values estimated from blockage corrections) for the non-blockage-corrected peak operating tip speed ratio, 2.33. The solid red line includes the theoretical fluctuating streamwise wave fluid velocity from the 2.5s period wave averaged over the turbine's height. It seems that the wave fluid velocity is increasing blade angle of attack beyond its stall angle for some rotations, explaining why the turbine would not operate at this tip speed ratio while this wave was present.

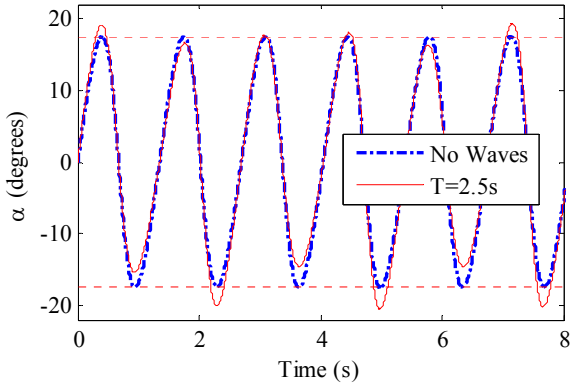

FIGURE 18. THEORETICAL TURBINE BLADE ANGLE OF ATTACK WITH 30% INDUCTION FACTOR IN A 2.5s PERIOD 0.15m HIGH WAVE AT λ=2.33.

Effects of Turbulence

PIV Experiments. To qualitatively observe the static stall delay phenomenon described by Swalwell et al. [12], A 36% solid grid with 3.18cm mesh size was placed 10 mesh widths upstream of a 7cm chord NACA 0012 hydrofoil in a 15.24cm square UNH water channel. The foil was placed at 9 degrees angle of attack in a 0.3m/s free stream velocity (Re_c=21,000). Flow was measured using high frame-rate stereo PIV. A photograph of the experimental setup is shown in Fig. 19.

FIGURE 19. WATER TUNNEL EXPERIMENTAL SETUP REGARDING DELAY OF STALL IN GRID TURBULENCE. FLOW IS FROM RIGHT TO LEFT.

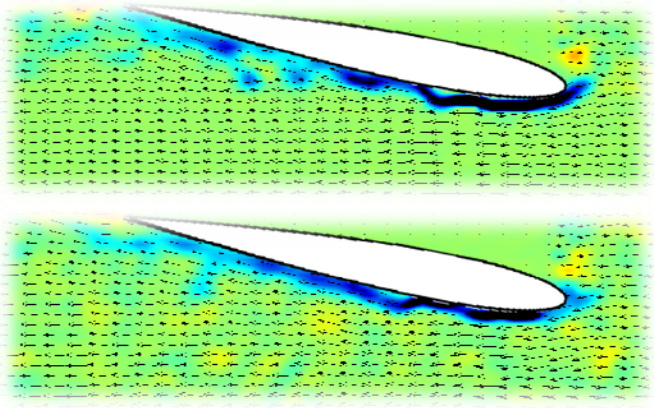

FIGURE 20. INSTANTANEOUS VELOCITY VECTORS FOR NACA 0012 HYDROFOIL AT α=9°, Re_c=21,000; FREE STREAM TURBULENCE LEVEL OF 1% (TOP) AND 5% (BOTTOM). BACKGROUND COLOR INDICATES IN-PLANE VORTICITY.

Preliminary sample results for the hydrofoil's instantaneous velocity and vorticity fields with streamwise turbulence levels of 1% (tunnel background turbulence) and 5% (with upstream grid) are shown in Fig. 20. In the higher turbulence case, the separation point seems to move towards the trailing edge of the hydrofoil, and the separated region becomes smaller, indicating a reduction in drag-inducing pressure on the lower surface.

GHT Performance in Grid Turbulence

The hydrokinetic turbine test bed was expanded to enable testing of turbines in grid turbulence. A turbulence generating grid was fabricated with a 36% solidity and mesh size of 6.4cm, placed 10 mesh widths upstream (10*M*) from the edge of the turbine blade sweep, shown in Fig. 21. The grid wire diameter Reynolds number at 1m/s is about 12,000, and the turbine location is between 10*M* and 25*M* downstream. A Nortek Vectrino+ Acoustic Doppler Velocimeter (ADV) was mounted approximately 5 mesh widths downstream from the grid, measuring velocity at a sample rate of 200Hz. Average turbulence intensities in the cross and streamwise directions were measured to be 23% at this location, confirming the finding of Groth and Johansson [16] that turbulence anisotropies quickly subside downstream of high Reynolds number, supercritical grids (i.e., the anisotropy measure v_{rms}/u_{rms} quickly converges to one). Upon further comparison to the results of [16], the turbulence intensities at the front edge of the turbine sweep (10*M* from the grid) should be approximately halved, or 11%. The grid turbulence will then experience a power law decay as described by Batchelor and Townsend [17]. However, here the decay of turbulence intensity is more complicated due to the induction exerted by the turbine, as well as the interaction with turbine blades, and will be less than that reported by [16].

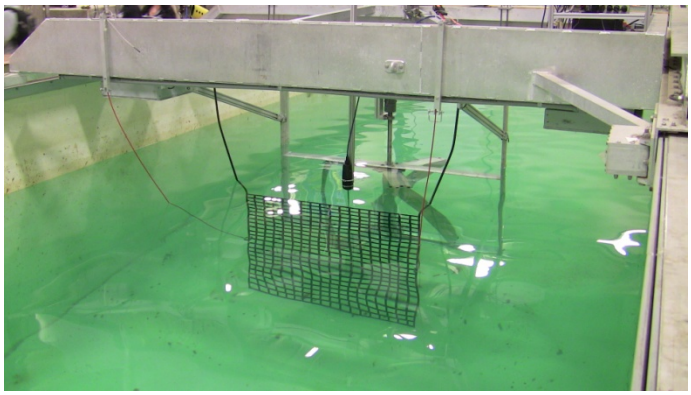

FIGURE 21. UNH-CORE HYDROKINETIC TURBINE TEST BED WITH GRID TURBULENCE GENERATOR INSTALLED.

Fig. 22 shows power coefficient plotted versus tip speed ratio for the GHT in grid turbulence. A larger range of tip speed ratios is observed, though their true value in turbulence is difficult to estimate. From ADV measurements at 5*M* without the turbine spinning, the average fluid velocity at the turbine in grid turbulence was estimated to be 0.87 times the carriage speed. Turbine tip speed ratio, power coefficient, and drag coefficient are all computed with this value, hence further measurement to gain more confidence regarding the mean velocity field encountered by the turbine downstream of the grid should be conducted. Despite the difficulty in comparing absolute values to the steady flow case, the shape of the plot in Fig. 22 shows a small decrease in power coefficient at high tip speed ratios and a slight increase for lower ones. This combined with the larger range of operating tip speed ratios suggests stall delay is occurring, though the effects are subtle.

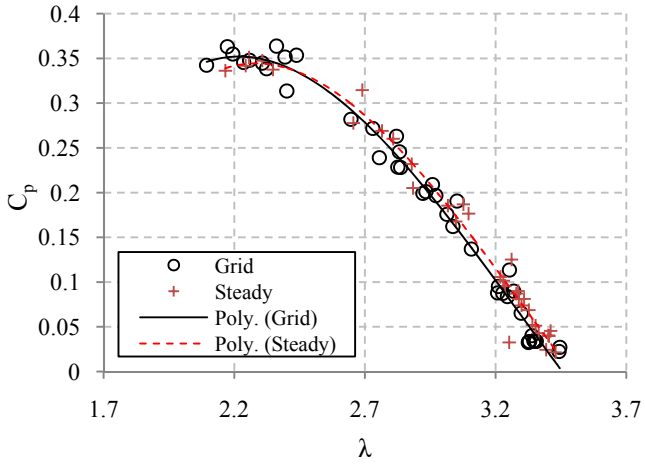

FIGURE 22. GHT POWER COEFFICIENT VERSUS TIP SPEED RATIO IN GRID TURBULENCE FOR U=0.9-1.1m/s.

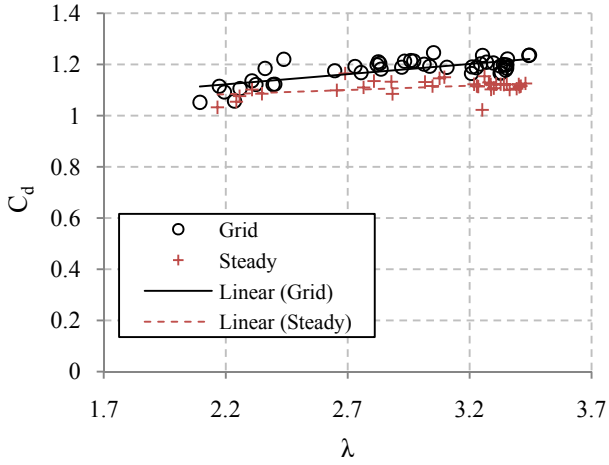

FIGURE 23. GHT DRAG COEFFICIENT VERSUS TIP SPEED RATIO IN GRID TURBULENCE FOR U=0.9-1.1m/s.

Fig. 23 shows the GHT drag coefficient in grid turbulence plotted versus tip speed ratio. The uncertainty in mean velocity at the turbine also makes comparison of turbine drag

coefficients in grid turbulence to steady flow difficult, but the slope of the trends seems to indicate turbulence more rapidly increasing drag coefficient at higher tip speed ratios.

CONCLUSIONS

The GHT was more effective than the LST at capturing hydrokinetic energy in a tow tank environment, with measured, blockage-corrected maximum power coefficients of 28% and 21%, respectively. The performance difference between the GHT and LST can be attributed partially to the LST's higher solidity and smaller average radius. The solidity also explains the lower operating tip speed ratios of the LST. Drag coefficients remain remarkably constant regardless of power extraction and the LST is in general a lower drag device.

Peak kinetic exergy efficiency for the GHT is 46% while only 35% for the LST. It would be interesting to see how these change for different blockage scenarios.

The GHT seems to be an effective converter for some of the kinetic energy within progressive surface waves. However, the presence of a wave limits the turbine's lowest operating tip speed ratio due to the wave's streamwise velocity fluctuation augmenting turbine blade angle of attack.

In isotropic homogeneous turbulence, the GHT power coefficient and drag coefficient curves slightly change shape. Relative to the non-turbulent case, power coefficients are slightly lower at high tip speed ratios and slightly higher at lower tip speed ratios. The range of operable tip speed ratios seems to increase in grid turbulence, possibly due to a delay of stall effect. Drag coefficient seems to increase more rapidly for higher tip speed ratios compared to the non-turbulent case.

Future work will include tows in larger scale turbulence, more akin to what a device would encounter in a real tidal or river flow.

ACKNOWLEDGMENTS

The work reported here was carried out at the Center for Ocean Renewable Energy at the University of New Hampshire (UNH-CORE), as part of the M.S. thesis of P. Bachant in Mechanical Engineering.

The authors gratefully acknowledge support from the offices of the UNH Vice Provost for Research and Dean of the College of Engineering and Physical Sciences, the UNH Mechanical Engineering Department, the New England Marine Renewable Energy Center for a Summer Research Fellowship, Lucid Energy Technologies, LLP and US Senator J. Shaheen and staff. The authors also thank A. Lightbody for the use of a Nortek Vectrino+ ADV.

REFERENCES

[1] Paraschivoiu, I., 2002. *Wind Turbine Design with Emphasis on Darrieus Concept*, 1st ed., Polytechnic International, Montreal, Quebec, Canada.

[2] Gorlov, A., 1995. "Unidirectional Helical Reaction Turbine". U.S. Patent No. 5,451,137, September.

[3] Gorlov, A., 1998. Development of the Helical Reaction Hydraulic Turbine. Final technical report. (DE-FG01-96EE 15669)

[4] Shiono, M., Katsuyuki, S., Kiho, S., 2000, "An Experimental Study of the Characteristics of a Darrieus Turbine for Tidal Power Generation". *Electrical Engineering in Japan*, 132(3), pp. 38-46.

[5] GCK Technologies, 2002-2006, Gorlov Helical Turbines, Production for Korea Ocean Research and Development Institute (KORDI) and testing by KORDI, Internal Reports

[6] Lee K., Yum K., Park J. and Park JW, 2009, "Tidal Current Power Development in Korea." Korean Ocean Research and Development Institute (KORDI), presentation at East Asian Sea Congress 2009 (EAS 2009), Philippines, November.

[7] Ocean Renewable Power Company, 2008, Status Report 4: OCGen Prototype Tidal Turbine Generator Unit Demonstration., June.

[8] Scientific American, 2010, "Testing the Waters with Tidal Energy", December.

[9] Schlabach et al., 2010, "In-Pipe Hydro-Electric Power System and Turbine", US Patent Application Publication, (Northwest Pipe and Lucid Energy), October.

[10] Manwell J., McGowan J., Rogers A., 2002, *Wind Energy-Explained*, John Wiley, UK.

[11] Dean, R., Dalrymple, R., 1991. *Water Wave Mechanics for Engineers and Scientists*, 1st ed., Vol. 2 of *Advanced Series on Ocean Engineering.* World Scientific, Hackensack, NJ, Chap. 4, pp. 79.

[12] Swalwell, K., Sheridan, J., Melbourne, W., 2001, "The Effect of Turbulence Intensity on Stall of the NACA 0021 Aerofoil". *14th Australasian Fluid Mechanics Conference*, 10-14, December, pp. 941-944.

[13] Sheldahl, R.E., and Klimas, P.C., 1981. Aerodynamic Characteristics of Seven Symmetrical Airfoil Sections Through 180-Degrees Angle of Attack for Use in Aerodynamic Analysis of Vertical Axis Wind Turbines. Sandia National Laboratories, Albuquerque, NM, March.

[14] Bahaj, A., Molland, A., Chaplin, J., Batten, W., 2007, "Power and thrust measurements of marine current turbines under various hydrodynamic flow conditions in a cavitation tunnel and a towing tank". *Renewable Energy*, 32(3), January, pp. 407-426.

[15] Schlabach, R. et al., 2010, Lucid Energy Technologies In-Conduit Hydro Power Testing at Utah Water Research Laboratory, Internal Report, Lucid Energy Technologies, December.

[16] Groth, J., Johansson, A., 1988, "Turbulence Reduction by Screens". *Journal of Fluid Mechanics*, vol. 197, May, pp. 139-155.

[17] Batchelor, G., Townsend, A., 1948, "Decay of vorticity in isotropic turbulence". *Proc. of R. Soc. London*, A 193, pp 539-558.